International Journal of Earth, Energy and Environmental Sciences
ISSN: 2517-942X
Vol:13, No:5, 2019

Numerical Simulation of Axially Loaded to Failure Large Diameter Bored Pile

M. Ezzat, Y. Zaghloul, T. Sorour, A. Hefny, M. Eid

***Abstract*—**Ultimate capacity of large diameter bored piles is usually determined from pile loading tests as recommended by several international codes and foundation design standards. However, loading of this type of piles till achieving apparent failure is practically seldom. In this paper, numerical analyses are carried out to simulate load test of a large diameter bored pile performed at the location of Alzey highway bridge project (Germany). Test results of pile load settlement relationship till failure as well as results of the base and shaft resistances are available. Apparent failure was indicated in this test by the significant increase of the induced settlement during the last load increment applied on the pile head. Measurements of this pile load test are used to assess the quality of the numerical models investigated. Three different material soil models are implemented in the analyses: Mohr coulomb (MC), Soft soil (SS), and Modified Mohr coulomb (MMC). Very good agreement is obtained between the field measured settlement and the calculated settlement using the MMC model. Results of analysis showed also that the MMC constitutive model is superior to MC, and SS models in predicting the ultimate base and shaft resistances of the large diameter bored pile. After calibrating the numerical model, behavior of large diameter bored piles under axial loads is discussed and the formation of the plastic zone around the pile is explored. Results obtained showed that the plastic zone below the base of the pile at failure extended laterally to about four times the pile diameter and vertically to about three times the pile diameter.

***Keywords*—**Ultimate capacity, large diameter bored piles, plastic zone, failure, pile load test.

I. Introduction

LARGE diameter bored piles are qualified to be the most powerful element of deep foundations implemented in many types of heavy loaded structures such as the high-rise buildings, offshore ports, wind power mills, storage silos, etc. They are employed most frequently both to support heavy loads and to minimize settlement [1], [2].

The in-situ full scale pile loading test is the most recommended methodology in several international geotechnical codes and foundation design standards [3]-[5] to determine the ultimate capacity of large diameter bored piles, and failure is defined in these codes by the uncontrolled settlement induced during the existence of ultimate load. In 1974 pile load test was performed at the location of Alzey highway bridge project (Germany) [6]. In this test a well instrumented large diameter bored pile was successfully loaded to failure. The necessity of this full-scale loading test was to accurately assess the ultimate bearing and friction capacities of the tested large diameter bored pile, in order to optimize securely and economically the foundation design of Alzey bridge. However, loading of large diameter bored piles till achieving apparent failure is practically seldom. This is attribu5ted to the significant amount of pile settlement that is usually required for the full mobilization of the pile shaft and base resistances [2], [7], [8]. Huge test loads and hence high-capacity reaction systems should be used to accomplish the required enormous settlements. Thus, the targeted failure load may not always be practical to achieve. This in most cases is the reason that the measured pile load-settlement curves for large diameter bored piles usually do not show an apparent failure point [2]. Therefore, various failure criterions have been proposed for interpreting the pile failure load (ultimate pile capacity) using the pile loading test data. Hansen [9], and Chin [10] techniques, among others are examples of different failure criteria proposed by several authors for this purpose. Unfortunately, variable degrees of uncertainty may be associated with these criteria's and hence seldom will any two give the same failure load [11].

Recently, numerical analysis has become a strong tool to simulate a lot of geotechnical problems. Numerical studies related to soil-structure interaction and axially loaded single pile are discussed by many authors [12]-[17]. Rarity of the available pile loading tests that achieved apparent failure was the main reason that the measurements of this well-documented Alzey bridge case history are utilized in many numerical studies performed by several researchers, e.g. [13], [17]. Despite of the interesting findings that were obtained in these studies, unfortunately due to the complexities of finite element method and limitations of the prepackage software's results of these numerical studies, an agreement with field measurements at the failure state was not shown. A back-analysis study was performed by [17] for the mentioned pile load test (alzey bridge case) and it was concluded that it is necessary to perform more back analyses of pile load tests to achieve better agreement with field measurements and give general recommendations.

The main objective of this research is to numerically study the behaviour of large diameter bored piles under axial compression loads, and to assess the pile ultimate capacity obtained from the numerical analysis using field measurement of axially loaded to failure pile load test (Alzey Bridge Case

M. Ezzat (Assistant Professor) is with the Department of Civil Engineering, Higher Institute of Engineering, Shorouk City, Cairo, Egypt (corresponding author, e-mail: m.ezzat@sha.edu.eg).

Y. Zaghloul (Assistant Professor) is with the Department of Structural Engineering, Higher Institute of Engineering, Shorouk City, Cairo, Egypt (e-mail: yzaghloul@yahoo.com).

T. Sorour (Assistant Professor) and M. Eid (Professor) are with the Department of Structural Engineering, Faculty of Engineering, Ain Shams University, Cairo, Egypt (e-mail: tamersorour2003@gmail.com, eidmona77@yahoo.com).

A. Hefny (Associate Professor) is with the Department of Civil & Env. Engineering, United Arab Emirates University, UAE (e-mail: a.hefny@uaeu.ac.ae).

Study). The established numerical model should well represent the field behavior of the tested pile in terms of total, bearing, and frictional ultimate capacities. Hence, this calibrated model can be utilized to investigate the large diameter bored pile failure mechanism.

II. In Situ Pile Loading Test

Sommer et al. [6] reported a full-scale well instrumented pile loading test for a single large diameter bored pile with diameter and length of 1.30 m and 9.50 m, respectively. This pile was installed in a homogeneous over-consolidated stiff clay soil layer with plastic limit of wp = 0.2, liquid limit of wl = 0.8 and water content of w = 0.22. The groundwater table was 3.5 meter below the ground surface. Average unconfined compressive strength (Qu) along borehole length was obtained as 300 kp/cm^2 (kilopond per square centimeter) as given in Fig. 1.

The reaction system used for the large diameter pile loading test consisted of main steel girders held with 20.0 m embedded length anchors. The compression anchors were at a horizontal distance of 4.0 m (three times of pile diameter) from the pile central loading axis as shown in Fig. 1. These anchors were also vertically extended to a depth between 15 and 20 m below the ground surface in order to ensure that anchors locations would not affect the skin friction and pile bearing results.

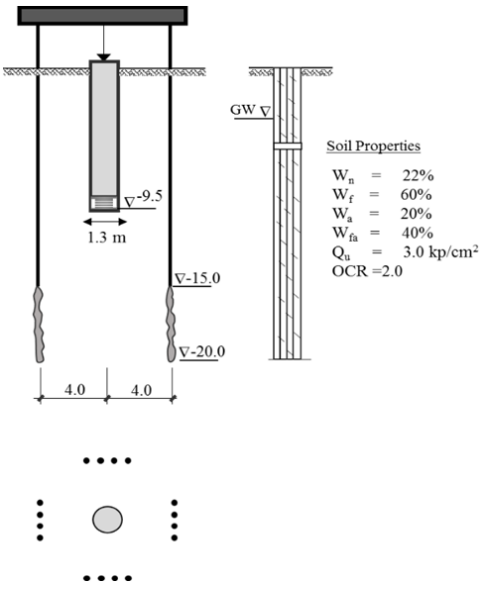

Fig. 1 Tests arrangement and typical soil profile with mechanical characteristics [6]

Large diameter bored pile was instrumented with an end bearing prefabricated concrete base contains load cell measuring device (Fig. 2). Also, settlement point devices with steel rods of 25 mm diameter were used to measure the settlement of neighbour soil near the pile. These settlement points were secured against the soil by plastic pipes, and were installed at a horizontal distance of 0.5 m, 1.0 m, 1.5 m, and 2.0 m from the pile's shaft at a depth of -0.50 m below ground surface, at the middle of the pile at level of -5.00 m and under the pile base at level of -10.00 m (Fig. 2). Pile settlement was measured using dial gauges at pile head level and also monitored using a concreted precision levelling device (0.1 mm).

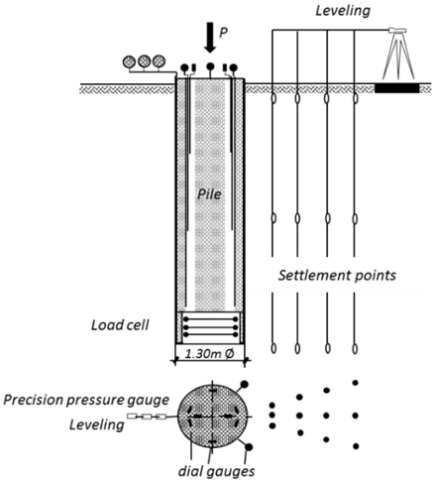

Fig. 2 Measuring devices and instrumentations [6]

A load measuring cells was placed immediately under the pile base. The difference between the load cell measurement and the applied load gave the load transferred by friction with the surrounding soil. Fig. 3 presents the measured pile settlement values using the dial gauges under each applied loading increment. Also, the respective values of bearing stress, unit skin friction, and the total applied pressure are given in the same figure.

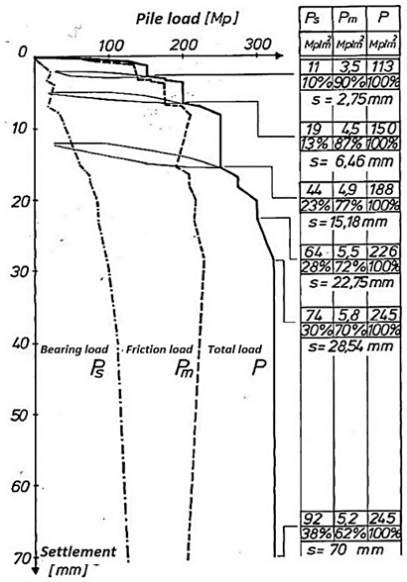

Fig. 3 In-situ measurements of the instrumented large diameter bored pile [6] * *Mp/m^2: mega-ponds per square meter*

III. Constitutive Models

The predicted response of the large diameter pile under axial

loads is investigated for three soil constitutive models. The models adopted are MC, SS, and MMC models.

The yield condition for the three models is developed based on coulomb's friction law of general states of stress. MC yield condition is controlled by the effective friction angle (ϕ') and the effective cohesion (c'). The dilatant behavior is represented through the dilatancy angle (ψ). Conversely, a cap type yield surface is introduced in the SS and the MMC models to simulate the irreversible strains due to primary isotropic compression. This yield cap describes an ellipse in the p'-q-plane. In the SS(SS) model the tops of all ellipses are located on a line with slope M that is not necessarily related to critical state as in the modified Cam-Clay model [18], but the modified cam clay model is obtained as a special case [19]. In the MMC model, a different cap is used where the top of the ellipses lies on the q-axis. Furthermore, yield criteria of the double hardening MMC model is represented by two yield surfaces, one for the shear yielding up to MC failure surface and another surface demonstrates the compression yielding [22].

Fig. 4 presents the three constitutive models stress strain relationships. As shown the MC model is an elastic perfectly-plastic model, while in the SS model, a logarithmic relation between the volumetric strain (ε_v) and the mean effective stress p' is introduced. The MMC model has a hyperbolic stress-strain relationship between the axial strain and the deviatoric stress. Fundamental to note that, the stiffness in the MC model is taken as constant value, while the stiffness in the SS and MMC model are stress dependent. The stress dependency for the MMC model follows the approach by [20], [21].

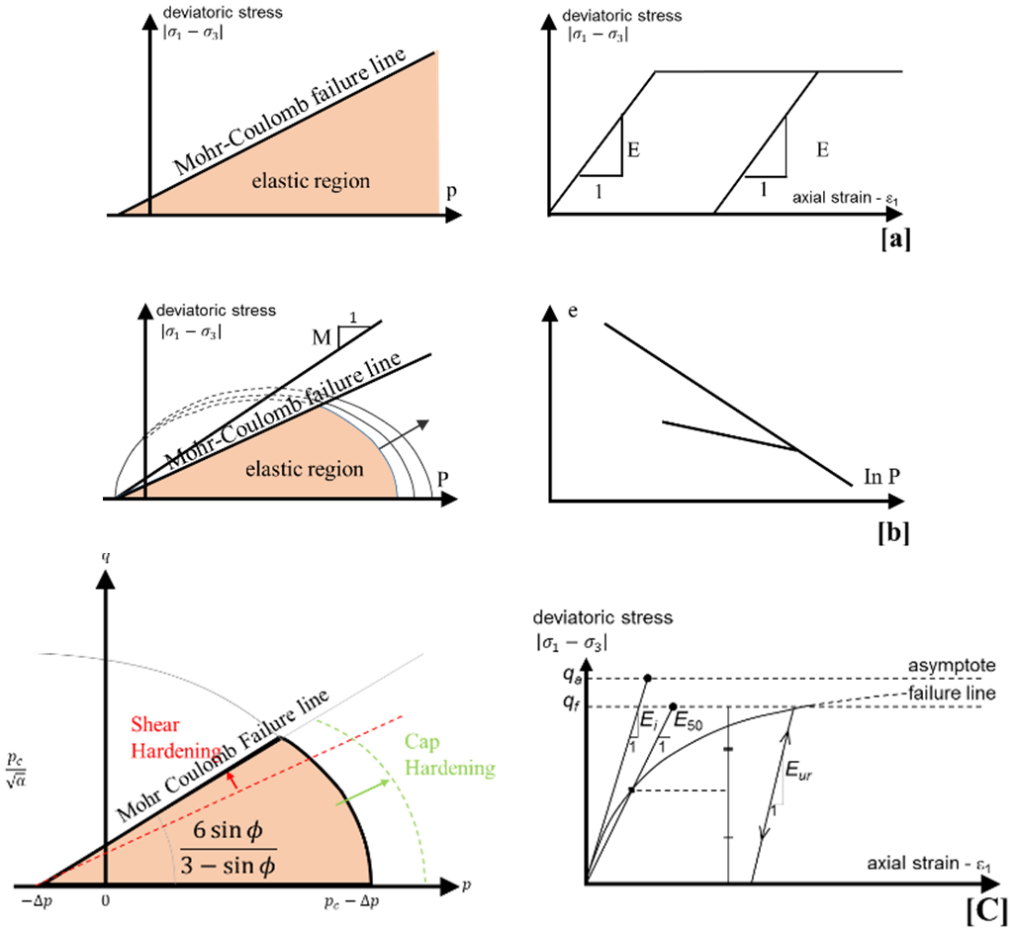

Fig. 4 Yield conditions and stress strain relationship for [a] MC, [b] SS(SS) and [c] MMC constitutive models

IV. Numerical Modelling

Axisymmetric two-dimensional numerical model has been established using GTS NX 2019. Based on a sensitivity analysis performed to eliminate the effect of model boundaries on the obtained results, model height of 40 m and width of 20m was adopted in the analysis (Fig. 5).

To avoid the numerical instability (singularity) of finite element model, the external boundaries were supported. The left and right sides were taken as fixed in the lateral-direction, and free to settle in the vertical-direction. Fixed supports are employed at the bottom boundary in both the horizontal and vertical directions, conversely top boundary was taken free.

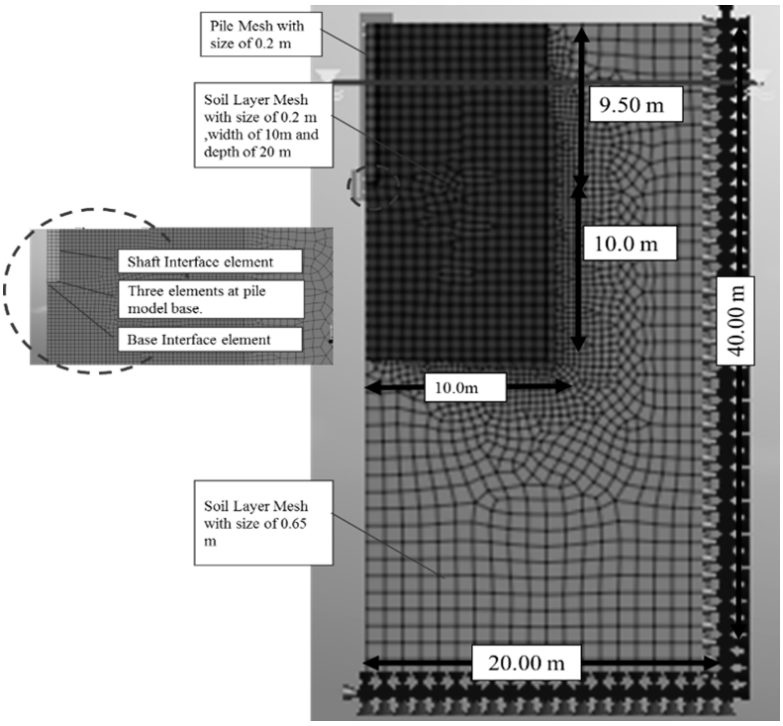

Fig. 5 2D axisymmetric finite element model

As shown in Fig. 5, quadratic high order elements (20-noded) were used to represent the soil. Three different mesh sizes were used to investigate the sensitivity of the soil mesh refinement and their effect on the results. Very good enhancement was noticed in both results of settlement and stress results when fine mesh (0.22 m) was utilized. However, time of the analysis was significantly increased. Results of these analysis attempts are not presented in this study due to the lack of space. As a compromise solution, a very fine mesh zone with size of 0.22 m was adopted around and under the pile (10 m x 20 m). Increasingly, soil mesh size is increased to be 0.65 m at external boundaries locations. As shown in Fig. 5, few triangular mesh elements were automatically generated due to the aspect ratio of the model geometry.

A. Soil Model Properties

Three constitutive models are used to simulate the soil. The first constitutive model is MC model, the necessary soil parameters for this model were adopted as given in [13] and the values are summarized in Table I. The second constitutive model is the SS model. The essential parameters for this model are taken according to [17] (Table I).

The MMC is recommended for simulation of the overconsolidated clay soil and dense sand soil by [22]. This Constitutive model simulates the soil material much precisely by considering three different values of elasticity modulus (E_{eod}, E_{50} and E_{ur}). The stress strain behavior for primary loading is highly nonlinear. As discussed in Sec. II, the in situ water content was measured as 22%, which is used to calculate the drained soil young's modulus (E_{eod}) using Fig. 6 [21]. The parameter E_{50} is the confining stress dependent stiffness modulus for primary loading. For small strain, E_{50} is used instead of the initial modulus that is more difficult to determine experimentally [22]. Also, another stress-dependent stiffness modulus (E_{ur}) is used to represent unloading and reloading stress paths. In several practical cases, it is appropriate to set E_{ur} equal two or three times the E_{50}, and to set E_{50} with value equals to the calculated value of E_{eod} [2], [23]. Soil shear parameters (c', ϕ') are taken as those for MC model.

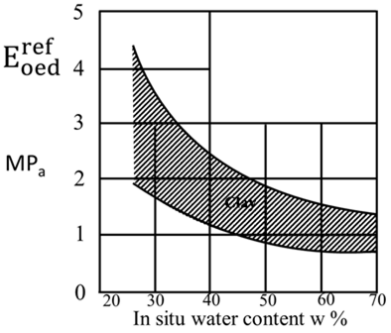

Fig. 6 Relation between clay soil in-situ water content, and the drained soil modulus of elasticity [21]

Soil lateral earth pressure coefficient (k_0) is calculated using the effective friction angle and overconsolidation ratio (1) according to [24]. Soil tensile strength is considered to be zero and also tension cut off is used in this analysis to avoid any soil tension results. Furthermore, very small value of dilatancy angle has been taken in soil material definition and dilatancy cut off option was activated.

$$K_0 = (1-\sin\emptyset)\ OCR^{\sin\emptyset} \quad (1)$$

The adopted values to define the over-consolidated stiff clay soil properties are summarized in Table I for the three utilized constitutive models (MC, SS, and MMC).

B. Pile Model Properties

Two-dimensional quadratic mesh elements (20-noded) are utilized to simulate the pile. Number of elements at pile base should not be less than two elements in order eliminate the mesh mesh dependency effect on pile bearing resistance, as reported by [17]. Consequently, mesh size of 0.216 m is adopted for the pile element. Elastic concrete isotropic material is utilized to define the pile mesh material. Characteristic compressive strength (*fcu*) of 300 kg/cm^2 was measured in side after 28 curing days [6]. Adopted properties of the pile are given in Table II.

C. Interface Element Parameters

Interface elements interact with two elastic-perfectly plastic springs which allow for differential displacements between the node pairs (slipping and gapping). First spring models gap while the second models slip. Slipping and gapping displacement at the interface is defined with (2) and (3) [25].

$$gap\ displacement = \frac{\sigma}{K_n} = \frac{\sigma.t_i}{Eoed_i} \quad (2)$$

$$slip\ displacement = \frac{\tau}{K_S} = \frac{\tau.t_i}{G_i} \quad (3)$$

where, $\mathbf{G_i}$: Shear modulus of interface [kN/m^2]. $\mathbf{E_{oedi}}$: Compression modulus of interface [kN/m^2]. $\mathbf{t_i}$: Interface virtual thickness (Ranges from 0.01 to 0.1) [-]. $\mathbf{K_n}$: Normal stiffness of interface [kN/m^3]. $\mathbf{K_s}$: Shear stiffness of interface [kN/m^3].

Shear and normal stiffness modulus of interface are determined according to the adopted soil modulus of elasticity for each of the three adopted constitutive models as given in Table III. On the other hand, MCcriteria is employed to distinguish between plastic and elastic response of interface. A strength reduction factor (R) is used to defined the shear properties of the interface elements on the shear strength of the neighbor soil layers as given by (4).

$$C_i = R^* C_{soil} \quad \tan\varphi_i = R^*\tan\varphi_{soil} \quad (4)$$
$$\psi_i = 0° \text{ for } R < 1, \text{ otherwise } \psi_i = \psi_{soil}$$

where; $\boldsymbol{\varphi_i}$: Angle of friction for the interface. [°], $\mathbf{C_i}$: Effective adhesion for the interface. [kN/m^2], $\boldsymbol{\psi_i}$. Angle of dilatancy for the interface [°].

The interaction between rough concrete surfaces and stiff clay soil, typical for bored shafts, was experimentally studied by [26]. For these evaluations, it was found that there is no considerable reduction for both friction angle and cohesion. In addition, several analysis attempts were performed in this study, and good agreement was obtained between field measured pile settlement values and finite element results, when the reduction factor of shear strength (R) was taken as 1.0 for interface elements.

TABLE I
OVER CONSOLIDATED STIFF CLAY SOIL PARAMETERS

Parameter	MC	MMC	SS	Unit
Type of material behavior	Drained	Drained	Drained	
Soil weight above/Below phr. Level (γ_{unsat}\ γ_{sat})	20	20	20	kN/m^3
Young's modulus (*E*)	60000	-	60000	kN/m^2
Poisson's ratio (*v*)	0.3	-	0.3	-
Secant stiffness (E_{50}^{ref})	-	45000	-	kN/m^2
Oedometer stiffness (E_{oed}^{ref})	-	45000	-	kN/m^2
Unloading-reloading stiffness (E_{ur}^{ref})	-	90000	-	kN/m^2
Power of stress level (*m*)	-	0.5	-	-
Unloading-reloading poisson's ratio (N_{ur})	-	0.2		-
Reference pressure (P_{ref})		100	-	kN/m^2
Power of stress level (m)		0.50		
λ			0.003	-
k			0.001	-
Cohesion (*c*)	20	20	20	kN/m^2
Friction angle (φ`)	22.5	22.5	22.5	°
Dilatancy angle (ψ)	0.0	0.0	0.1	°
Lateral earth pressure coeft. (K_0)	0.80	0.80	0.80	-
Soil Tensile Strength	0.0	0.0	0.0	kN/m^2

TABLE II
LARGE DIAMETER PILE STRUCTURAL PARAMETERS

Pile Material	Concrete	Unit
Pile Diameter (D)	1.30	m
Pile Length (L)	9.50	m
Young Modulus (E elastic)	24248711	kN\m^2
Poisson's Ratio (μ)	0.20	[-]
Unit weight (γc)	24.0	kN\m^3

TABLE III
INTERFACE ELEMENTS PARAMETERS

Parameter	MC	MMC	SS	Unit
Interface nonlinearity	Coulomb Friction	Coulomb Friction	Coulomb Friction	
Interface Adhesion (Ca)	20	20	20	kN/m^2
Interface Friction angle ($Ø_i$)	22.5	22.5	22.5	°
Interface Dilatancy angle (¥i)	0	0	0.1	°
Shear stiffness modulus (K_t)	250000	375000	250000	kN/m^3
Normal stiffness modulus (K_n)	2750000	4125000	2750000	kN/m^3
Tensile Strength	0	0	0	kN/m^2

V. STAGES OF ANALYSIS

The analysis is divided into three stages [2], the first stage represents the initial stresses of the soil before pile implementation. Second stage starts with changing the pile volume to concrete material as a replacement of soil material. At this stage, rigid interface elements are used to connect pile and soil mesh elements in order to avoid any numerical instability (singularity) [25], [2], and pile own weight is considered at this stage. The calculated deformations of the first and second stages of analysis are discarded in order to start to account for pile settlement due to applied loads only. Interface elements are activated in the third stage of analysis, and the rigid interface elements are deactivated. Load of 4000 kN is also applied on the pile head in the third stage. Load is implemented using incremental loading steps to simulate the

pile loading sequence with same field loading test steps (see Fig. 3).

VI. Results and Analysis

Fig. 7 compares between field measurements of pile load settlement and the obtained results of the three performed numerical analyses using three different soil constitutive models (MC, SS, and MMC). It can be seen that good agreement is obtained at the initial working loads (up to 1500 kN) between field measurements and numerical results of the three utilized constitutive models. At higher loading levels (2000 kN) differences were found between the three numerical models results, as SS model results showed stiffer behavior compared to MMC and MC models results.

According to the case study, failure load was measured as 3250 kN. At this load pile settlement was measured as about 29 mm and suddenly increased to 70 mm at the same load. Pile settlement is also determined at load 3250 kN to be about 33 mm (2.5%D) and 42 mm (3.23%D) according to results of SS and MC models respectively. On the other hand, 70 mm (5.38%D) is the result that obtained for pile settlement at load of 3250 kN when MMC model (MMC) is used. This result highlighting that good agreement with field measurements is obtained at load of 3250 kN. Worth noting that pile settlement is obtained as 31 mm at load of 3000 kN and increased to be 70 mm under load of 3250 kN (the failure load).

Fig. 8 presents the finite element result (MMC) of the deformed shape for soil and pile, under the failure load of 3250 kN.

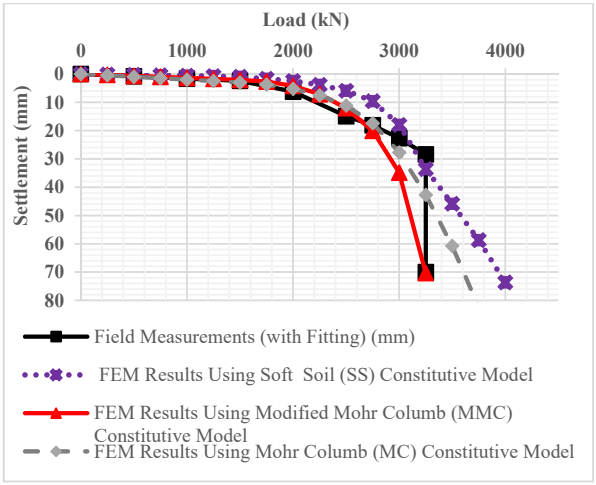

Fig. 7 Comparison between field measurements and pile load settlement results obtained from the three numerical models with different constitutive models simulating the soil

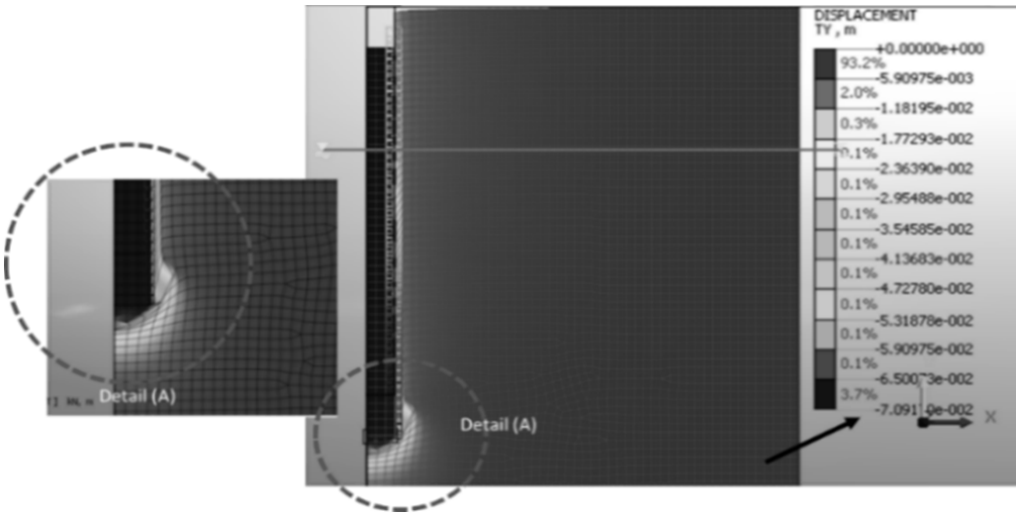

Fig. 8 Deformed shape of the finite element mesh (MMC) under load of 3250 kN (Failure load)

Large diameter bored pile load transfer mechanism is obtained by determining the pile bearing load at each loading increment utilizing the obtained bearing stress at pile base level. Pile friction resistance are calculated by deducting the bearing load from total applied load at each loading increment. Relations between pile load settlement, pile friction and bearing capacities under each loading increment are obtained for the three numerical models.

Figs. 9-11 respectively compare between the obtained numerical results using the three models (MC, SS and MMC) and the field measurements. The comparisons are shown in the form of pile load transfer curves, as the relation between total applied load, friction resistance, bearing resistance and pile settlement is obtained for the three numerical models and compared with field measurements. It is obvious from these figures that MMC model is superior to the other two models (MC and SS), due to its success to obtain closer results to field measurements for each of the pile total, bearing and friction resistances. Furthermore, differences between the obtained total and bearing resistances from the three numerical models are highlighted in Fig. 12. On the other hand, the three model's results of the pile friction resistance are compared in Fig. 13.

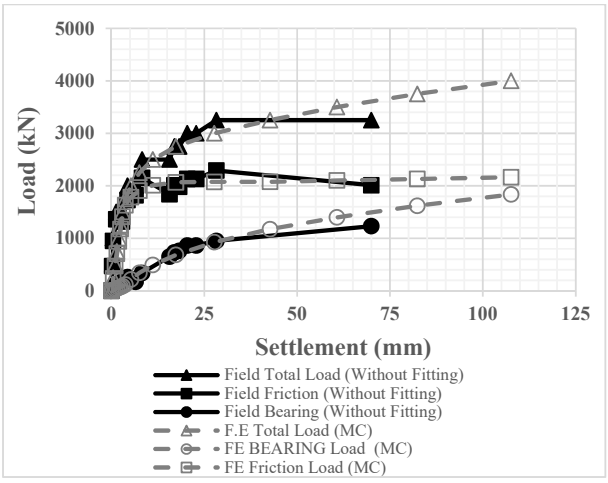

Fig. 9 Comparison between field measurements and finite element results of pile bearing, friction, total load and settlement for the MC

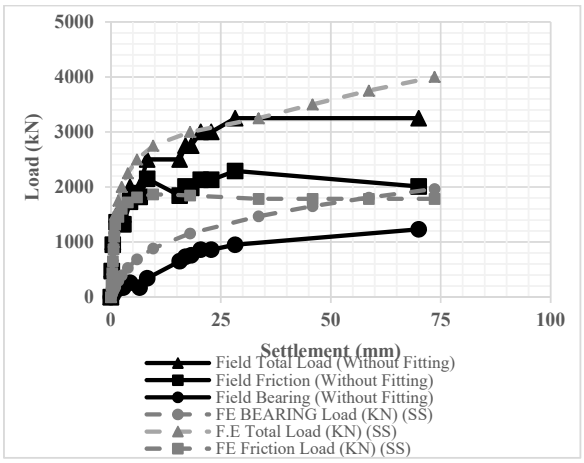

Fig. 10 Comparison between field measurements and finite element results of pile bearing, friction, total load and settlement for the SS

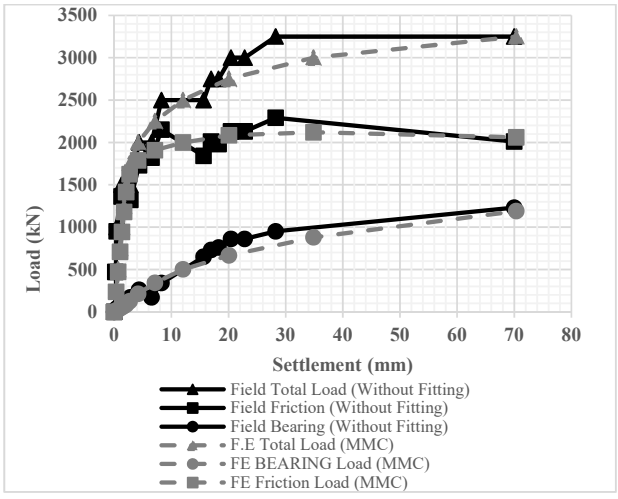

Fig. 11 Comparison between field measurements and finite element results of pile bearing, friction, total load and settlement for the MMC model

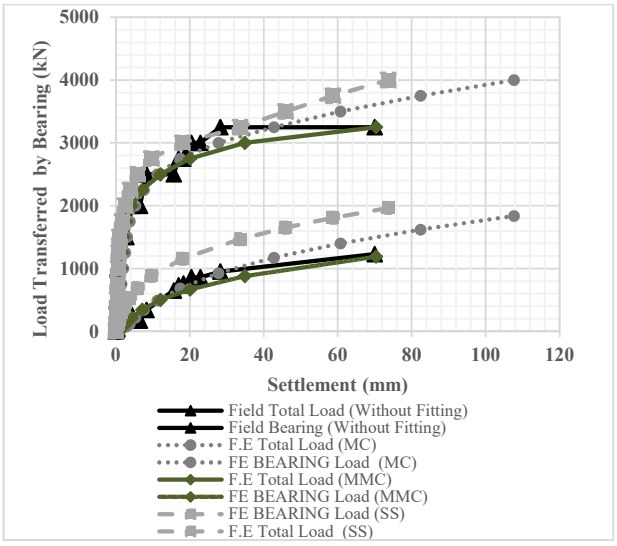

Fig. 12 Comparison between obtained total and bearing resistances using the MC, SS, and MMC models

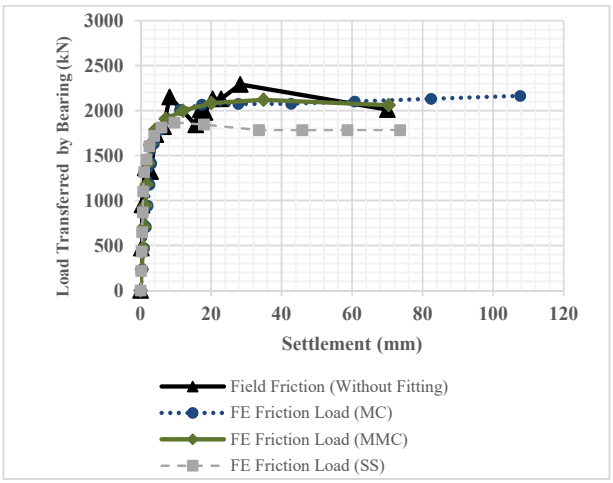

Fig. 13 Comparison between obtained friction resistances using the MC, SS, and MMC models

Fig. 12 pinpointed that SSmodel produced greater value for pile bearing resistance than those obtained from the other two numerical models. Almost the same values of pile bearing resistance are obtained from MMC and MC numerical models up till load of 2750 kN. After this load, base resistance results obtained from MC model seems to be much stiffer than those obtained using MMC numerical model. However, at the failure load of 3250 kN, good agreement was only obtained between MMC results and field measurements.

The difference between the three model's bearing resistance results is attributed to the different formulation of the oedometer stiffness in the three models [17]. As, in the MC model a constant stiffness is considered, while in the SS and the MMC models stiffness is stress dependent. This stress dependency is linear for the SS model and parabolic for the MMC model. As a consequence, the stiffness of the MMC and the SS models is the

same for a vertical stress of 100 kPa. For higher stresses E_{oed} is higher in the SS model than in the MMC model. Consequently, SS model obtains a higher base resistance as presented in Fig. 12. On the other hand, friction resistance results of the three models tend to linearly increase up till applied load increment of 1500 kN (working load), and the full friction mobilization is achieved at load increment of about 2500 kN for the three models (Figs. 9-11). The obtained pile settlement value at the full mobilization load (2500 kN) is about 20 mm for the three models which represents about 1.5 % of the pile diameter (1.30 m).

Fig. 13 demonstrates that the peak value (2070 kN) obtained for friction resistance from three models are almost near equal. However, the shape of the friction resistance curve of MCmodel seems to be consistent with its yielding criteria as it linearly increased to achieve its peak value then tends to be constant (Elastic- Perfectly plastic). In contrast, the SSmodel friction resistance curve showed slightly decrease after peak then tend to be constant. Also, For the MMC model, the shape of the friction resistance curve is hyperbolic. It was also observed that the difference between the maximum obtained friction resistance value (Peak) from the three models, is less than the difference between their bearing resistance results (see Fig. 12). This may be attributed to the usage of interface elements. As, the MCcriterion (5) is used in the three model's interfaces to distinguish between elastic and plastic behavior. In the three models, the same interface shear parameters (ϕ_i and C_i) are adopted.

$$|\tau| = \sigma_h \tan \varphi_i + c_i \quad (5)$$

Furthermore, interest of the pile load transferred by friction is significantly decreased after achieving the full mobilization as shown in the results of the three models (Fig. 13). The full mobilization means that the transferred shear stresses from the pile shaft become equal to the soil shear strength (τ) according to the defined values of the interface cohesion (c_i) and friction angle (φ_i). So that only the change in the stresses ($\boldsymbol{\sigma_h}$) around the pile shaft may be the responsible factor of the decrease in friction resistance results after the full mobilization. This expectation will be widely investigated in upcoming sections.

Based on the results presented in this section, it is clear that the MMC well represents the field behavior of the tested pile in terms of total, bearing, and frictional capacities. In the following sections, based on the calibrated MMC model, the load transfer and the failure mechanism are discussed.

VII. Large Diameter Bored Pile Load Transfer

Axial load distribution along pile shaft length is calculated at each loading increment by multiplying the vertical normal stress in the shaft by pile cross sectional area (Fig. 14). It is worthwhile noting that pile load values at the base level were calculated by integration of bearing stresses at the pile base.

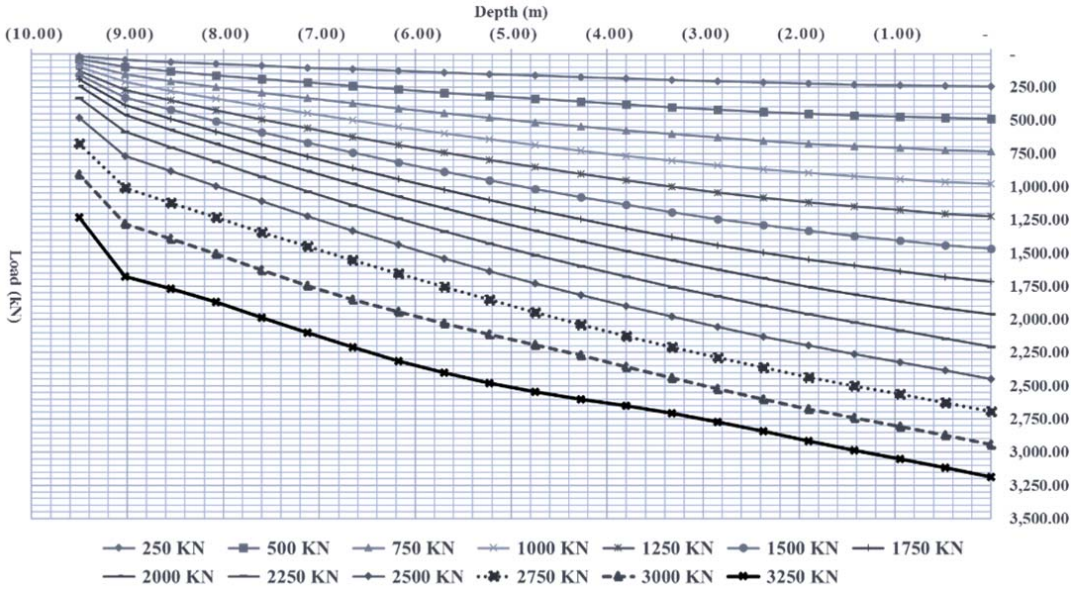

Fig. 14 Calculated pile axial load distribution with depth using finite element method

Interaction between pile base and soil is investigated by calculation of the pile bearing load percentage of total applied load at each loading increment ($Q_{bearing}/Q_{total}$). Fig. 15 compares between finite element results of bearing load percentage and the field measurements at every loading increment. Similarly, pile friction load percentage of the total applied load ($Q_{Friction}/Q_{Total}$) was calculated at each loading increment using both of the numerical results and field measurements and the result are shown in Fig. 16.

It can be seen from Fig. 15 that, good agreement is obtained between field measurements and finite element analysis results, also the percentage of transferred load by bearing was very small (about 5%) at the initial loading increments, then increased to be about 10% of the total applied load at the

working load (1500 kN). The induced settlement at the working load was only 2.75 mm.

Significant increase is observed in the percentage of the transferred load by bearing after applied load of 2000 kN, as it achieved about 26% of the applied load at load of 2500 kN. Fundamental to note that the full friction mobilization occurred at load of 2500 kN (see Fig. 11). These observations may explain the obvious increase in pile settlement at this stage, as at load of 2500 kN, pile settlement increases to be about 16 mm.

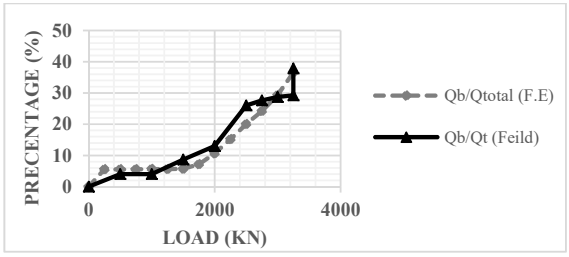

Fig. 15 Comparison between field and finite element pile bearing load percentage of total applied load ($Q_{bearing}/Q_{total}$)

Fig. 16 reveals that good agreement is also obtained between field measurements and finite element analysis results. Also, total applied load was predominantly carried by friction at the initial loading increments of (250, 500, and 1000 kN), as percentage of the transferred load by friction at this stage is about 95% of the total applied load. Although pile settlement value was small (1.3 mm) but it was enough to activate the soil friction resistance. At the working load (1500 kN), percentage of the transferred load by friction decreased to be about 90%, also it was observed that pile settlement is increased to be about 2.75 mm at this load. Obvious decrease is noticed in friction load percentage after load increment of 2000 kN, as it decreased to 72% at load of 3000 kN. Pile settlement increase was also observed at this phase, as settlement increased from 6.46 mm at load of 2000 kN to 22.75 mm at 3000 kN.

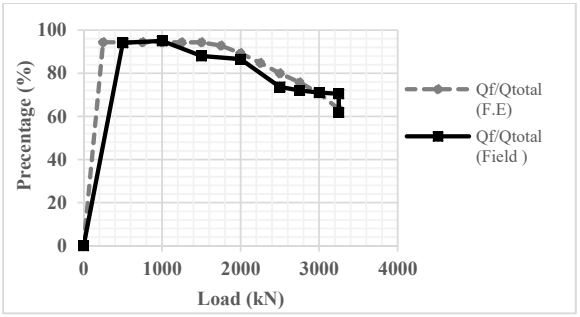

Fig. 16 Comparison between field measurements and numerical results of pile friction load percentage of total applied load ($Q_{friction}\backslash Q_{total}$)

At applied load of 3000 kN, bearing load percentage of about 30% is obtained. This percentage is increased to be about 38% at the last load increment (3250 kN, failure load). It is worthwhile noting that only 8% increase in percentage of the transferred load by bearing was enough to increase the induced settlement from 28.54 (at 3000 kN) to be 70 mm at the last load increment (failure load). This was described as an apparent failure according to the case study.

VIII. Skin Friction

Tangential stresses of the interface elements in vertical direction (Y-Axis) is determined from the calibrated numerical model at each load increment along the interface length. The relation between interface tangential stresses and depth is shown in Fig. 17. These tangential stresses represent the soil unit skin friction distribution along the pile shaft at each load increment.

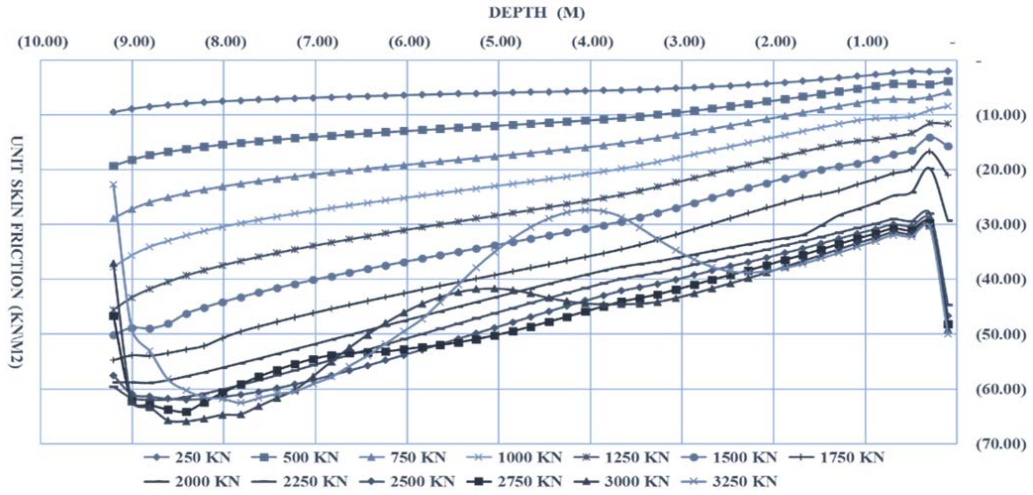

Fig. 17 Average values of unit skin friction obtained using finite element method through the tangential stress at interface element

Generally, at the full mobilization load (2500 kN), unit skin friction results tend to achieve the value of the considered effective cohesion (c') at the ground surface level, and gradually increased with depth with slope equals (tan Ø'). The obtained

shear stress value at this load equals the soil shear strength according MC criterion (5) directly above the pile base level, which confirming that full friction mobilization occurred at this load.

It was also noticed that at the last three loading increments significant increase in skin friction occurs at the ground surface level. The same observation was also reported by [27], as they observed a large increase in lateral earth pressure coefficient at the ground surface in several performed axial pile loading static tests. This may be attributed to the dilation effects near the ground surface where the confining pressure is low compared to deeper depths.

Fig. 17 also showed that unit skin friction values tend to decrease after load increment of 2500 kN (Full mobilization) at the last three applied load increments (2750, 3000 and 3250 kN). This decrease may be attributed to the arching action effect according to [28], [29] explanation (Fig. 18). To investigate the change in soil stresses after the full mobilization the relation between soil vertical and horizontal stresses with depth was plotted at the initial condition (Fig. 19 (a)), and after the full mobilization at load of 2500 kN (Fig. 19 (b)). Also, lateral earth pressure coefficient value was calculated for both cases as shown in Fig. 19 (c).

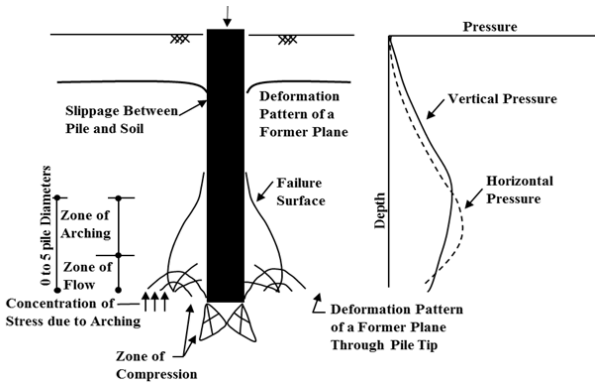

Fig. 18 Change of the stresses around the Pile and at the tip due to arching action [29]

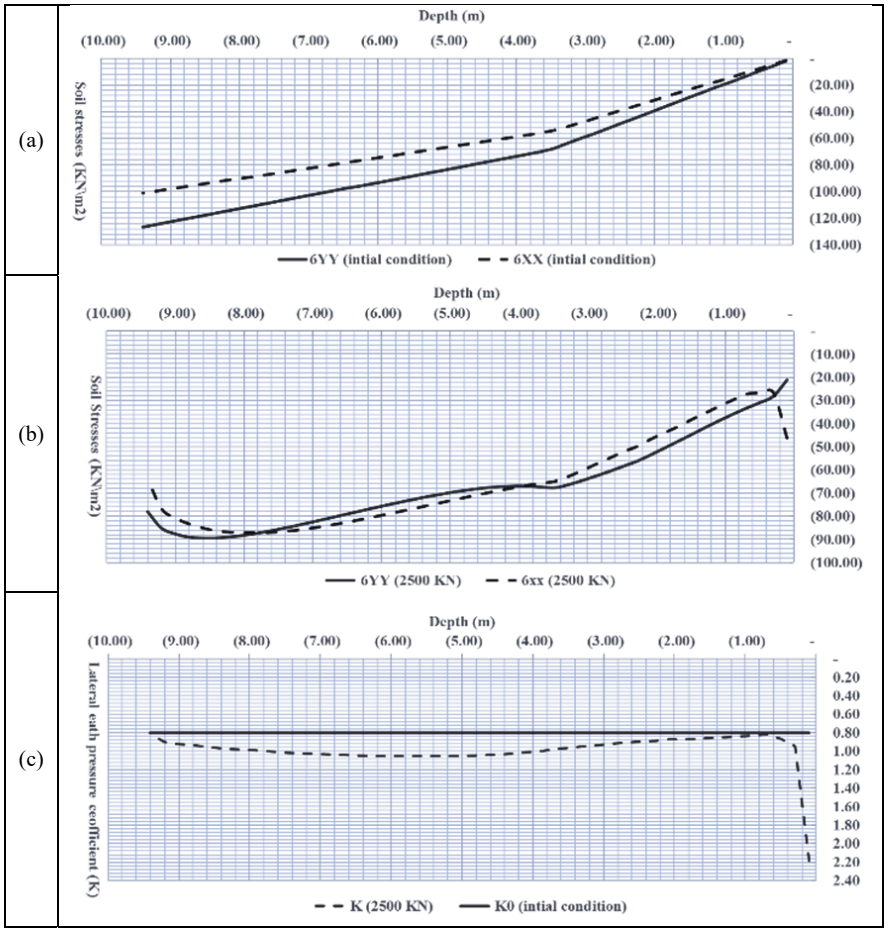

Fig. 19 Finite element results soil stresses distribution with depth, directly beside pile element. (a) soil vertical and horizontal stress distribution with depth at the initial condition. (b) soil vertical and horizontal stress distribution with depth under load of 2500 kN (after full mobilization). (c) lateral earth pressure coefficient at the initial condition (K_0) and under load of 2500kN (K)

It can be seen from Fig. 19 (b) that the horizontal stress values are consistent with the obtained skin friction values

presented in Fig. 17. Also, soil horizontal stress values were less than vertical stresses values at the upper zone of the pile shaft length above level of -4.0m below ground surface.

At distance between 4.0 m below the ground surface and of about 3.0 m (H/3) above the base the soil horizontal stresses were observed to be greater than the soil vertical stresses. These results agree with [29] observations related to arching action (Fig. 18).

Furthermore, both vertical and horizontal stresses decreased at pile base level which explaining the decrease in unit skin friction results at pile base level after full mobilization (see Fig. 17).

The distribution of lateral earth pressure coefficient (K) value around the pile at full mobilization of side resistance (applied load 2500 kN) is shown in Fig. 19 (c). As can be seen at full mobilization of side resistance, K values along the pile are greater than the at rest initial value (0.8) except at the base of the pile where a value equal to the at rest value was observed. The largest values of K were observed near the ground surface. This is in agreement with observations made by [1] and [27] as discussed before.

IX. Size of Plastic Bulb under Pile Base

The formed plastic points at each load increment is obtained from the calibrated numerical model as summarized in Figs. 20-34.

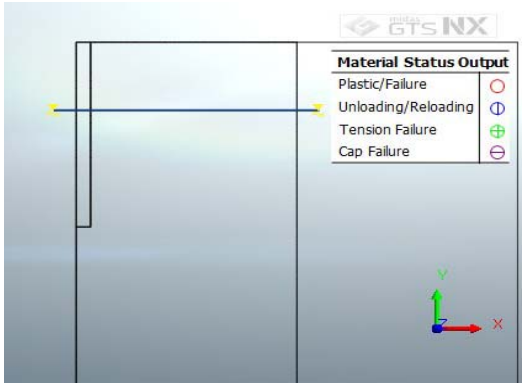

Fig. 20 Formed plastic points at the initial stage

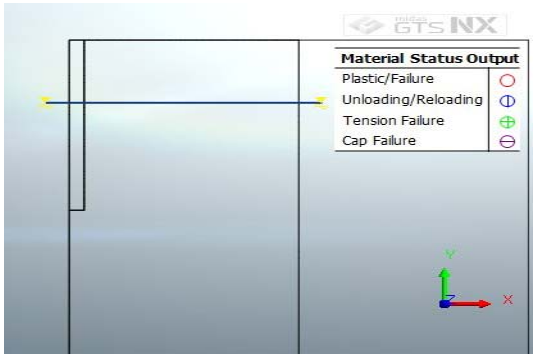

Fig. 21 Formed plastic points at the second stage (concreting)

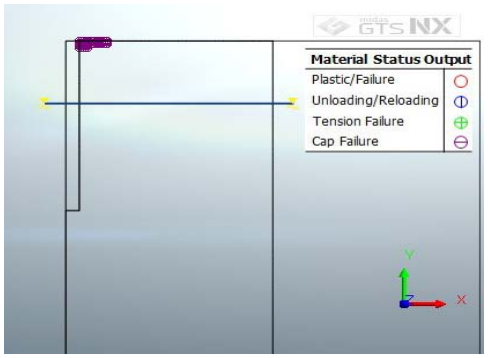

Fig. 22 Formed plastic points under load of 250 kN

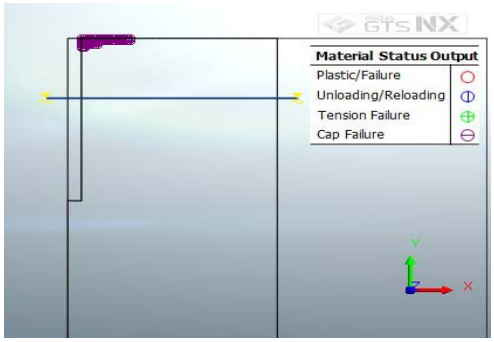

Fig. 23 Formed plastic points under load of 500 kN

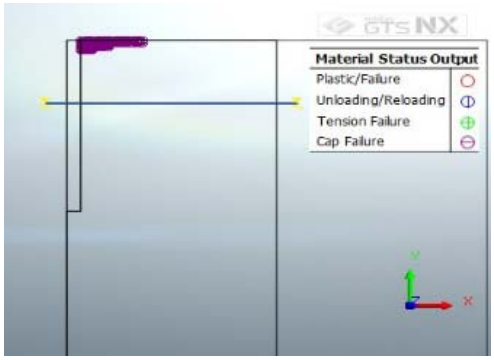

Fig. 24 Formed plastic points under load of 750 kN

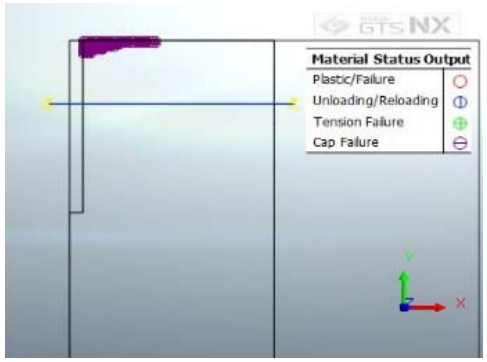

Fig. 25 Formed plastic points under load of 1000 kN

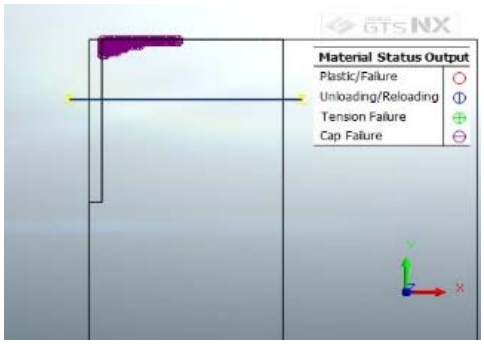

Fig. 26 Formed plastic points under load of 1250 kN

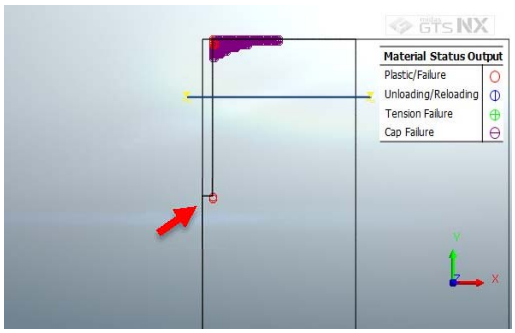

Fig. 27 Formed plastic points under load of 1500 kN

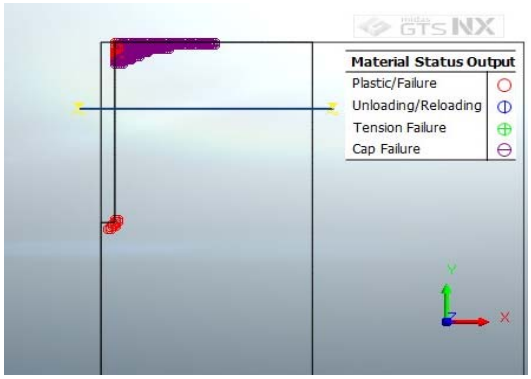

Fig. 28 Formed plastic points under load of 1750 kN

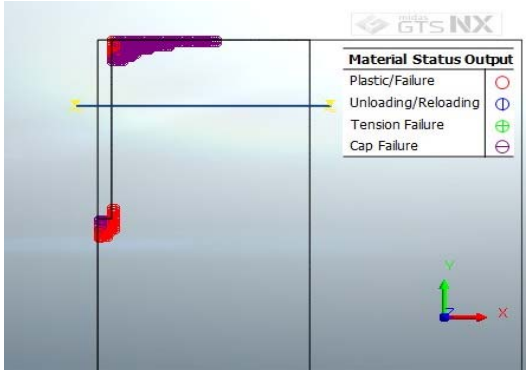

Fig. 29 Formed plastic points under load of 2000 kN

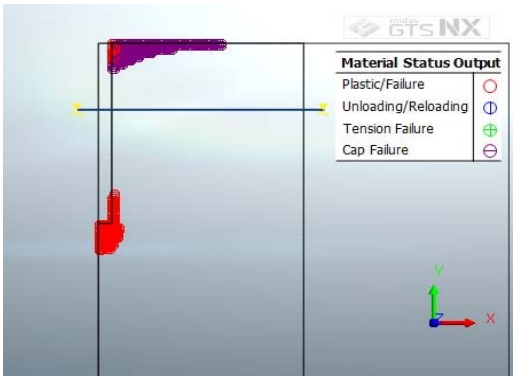

Fig. 30 Formed plastic points under load of 2250 kN

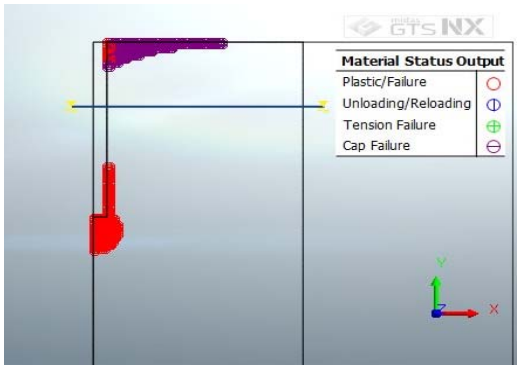

Fig. 31 Formed plastic points under load of 2500 kN

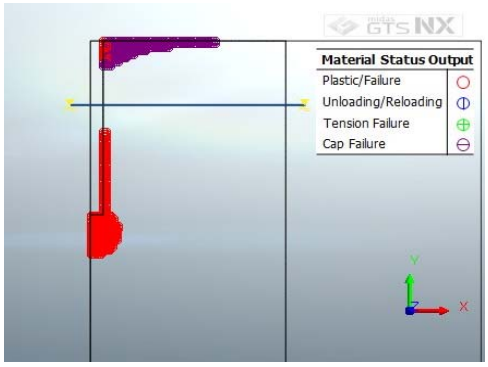

Fig. 32 Formed plastic points under load of 2750 kN

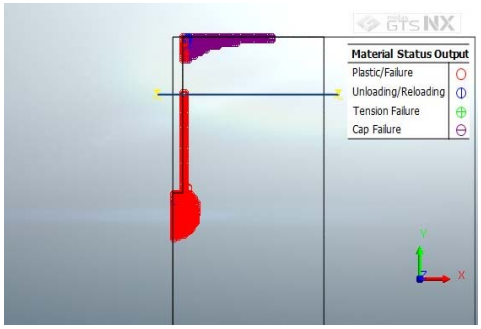

Fig. 33 Formed plastic points under load of 3000 kN

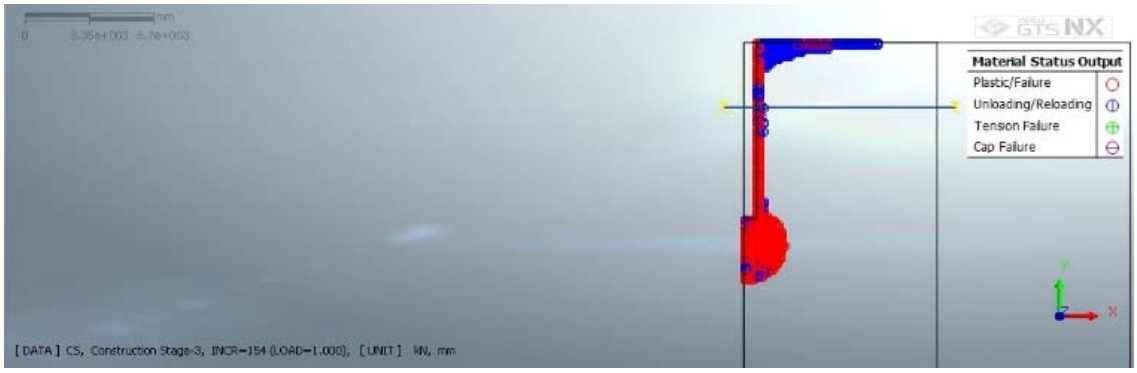

Fig. 34 Finite element results of the Formed plastic points under load of 3250 kN (Failure load)

It can be seen from these figures that the formation sequence of the plastic points around and below the pile shaft is consistent with pile load transfer mechanism presented in pervious sections. As shown in Figs. 20-26 (Load increment 0 to 1250 kN), plastic points are only formed around the pile head which agrees with field measurements and numerical results of pile load transfer, as load was predominantly (95%) transferred by friction at the initial load increments (Fig. 16). Fig. 27 indicates that the first initiation of plastic points around pile base was under load of 1500 kN. This result is also consistent with pile load transfer results shown in Fig. 16, as the interest of transferred load by bearing was increased at this load (1500 kN). Plastic points fulfilled the zone around pile base when load increased to 2500 kN (Fig. 31). This result agrees with skin friction results shown in Fig. 17 as the transferred shear stresses increased to be equal soil shear strength at pile base level under this load increment (2500 kN).

At load of 3000 kN (Fig. 33), the first unloading\reloading point is formed which may be attributed to the large settlement value (25.5 mm) at this load and to the slippage between soil and interface element that may cause a stress relief at soil near ground surface (Fig. 34). At the failure load of 3250 kN, Fig. 34 pinpoints the significant increase in plastic bulb size under pile base. As shown, plastic points extended and covered the whole interface length which indicates that the full friction and bearing mobilization occurred and also reveals to failure existence. Furthermore, using engineering drawing software dimensions of the plastic bulb has been measured in both diameter and length above and below the pile base. Fig. 35 demonstrates the size and length of formed plastic bulb at each loading increments.

It can be seen from Fig. 35 that plastic bulb starts to form at pile base with small diameter at load of 1500 kN. Plastic bulb size obviously increased to 2.34 D at load of 2500 kN (80% of the failure load) and achieved a maximum diameter of 3.73D (about four times of pile diameter) under failure load (3250 kN). Moreover, plastic points extended in length above and below pile base level as the axial load increased. As shown in Fig. 35, very small length of plastic points was measured below and above base under working loads (250 - 1500 kN). An increase in plastic bulb length is noted with load increase to be about one and half times the pile diameter at load of 2500 kN. It should be noted that plastic points extended above pile base for a length of about five times the pile diameter at load of 3000 kN (5D). At failure load of 3250 kN plastic points covered full interface length (9.50 m) and extended for a length nearly equal to three times of pile diameter below the pile base level (3D).

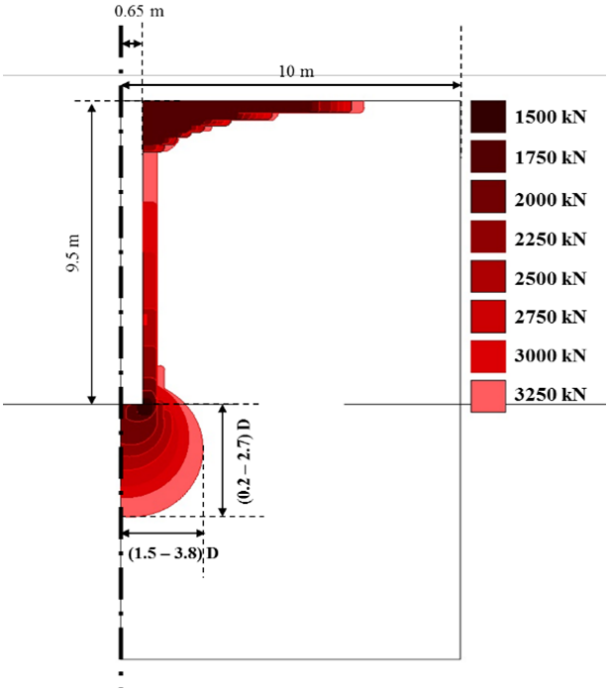

Fig. 35 Propagation of plastic bulb diameter with loading

The formation sequence of the plastic points can also describe the response of large diameter bored pile in this overconsolidated clay soil. This large diameter bored pile passed through three main stages to achieve the induced large settlement at the failure state. These three phases can be classified into the elastic phase, the mobilization phase, and the failure phase. Fig. 36 summarizes the response of this large diameter bored pile at each stage.

In the elastic phase, the interaction between soil and pile is close to be linear elastic. The applied load is predominantly transferred by friction in this stage (about 95% of the total applied load). No plastic points are detected in this phase. At the

mobilization phase, an obvious increase in the pile settlement rate is noticed in the field measurements and numerical results. The percentage of the load transferred by bearing is increased in this phase (Fig. 15). The soil skin friction is also increased to achieve its peak value of the soil shear strength (Fig. 17) at pile settlement of 1.5% D (Fig. 11). Plastic zones are formed at the pile base and vertically extended to a large part of the shaft (Fig. 31). In the failure phase, applied load is predominantly transferred by bearing, and the pile load transferred by friction tends to be constant (slightly decreased) (Fig. 11). Apparent failure is observed through the large induced pile settlement at the end of this stage (Fig. 7). The plastic points are existed at the base and covered almost the whole length on the pile shaft (Fig. 34).

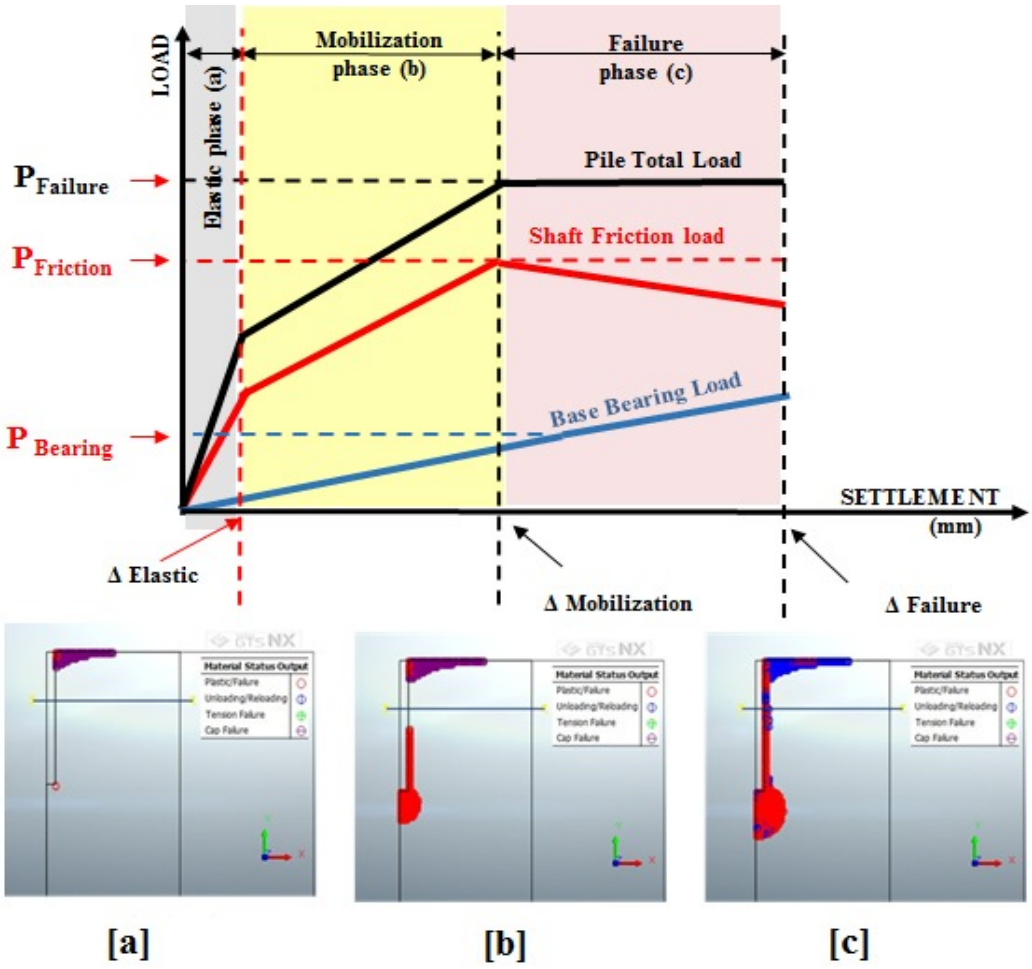

Fig. 36 Schematic diagram of three phases that large diameter bored pile passing through to achieve the failure. (a) Elastic Phase, (b) Mobilization Phase, (c) Failure Phase

X. Conclusions

Based on the numerical study conducted, the following conclusions are drawn:

- Very good agreement was obtained between field measurements and numerical results for the load settlement relationship and load transfer by friction and bearing.
- Both of the field loading test measurements and numerical results revealed that the ultimate capacity of the large diameter bored pile in overconsolidated stiff clay was 3250 kN, and the pile settlement induced at the ultimate load was 70 mm.
- Numerical analysis is capable of simulating the behavior of large diameter bored pile when the appropriate soil model is carefully selected.
- MMC constitutive model is superior to MC, and SS models in simulation of the drained condition of the over consolidated stiff clay soil.
- The numerical model results revealed that about 90% of the total applied load was predominantly carried by friction at the initial loading increments (working loads), and only about 10% of the total applied load was carried by pile bearing resistance. However, at ultimate load, friction resistance is 62%, and bearing resistance increased to 38% of the total applied load.
- After the full friction mobilization state, lateral earth

pressure coefficient (K) reached greater value near ground surface and lower value (equals its initial value K_0) at pile base level.

- Arching action at the pile base causes a change in both soil vertical, and horizontal stresses around the pile, after the full friction mobilization.
- Soil passed through three main stages to achieve the induced large settlement of the large diameter pile at the failure state. These three phases can be classified into the elastic phase, the mobilization phase and the failure phase;
- In the elastic phase, the interaction between soil and pile is close to be linear elastic. The applied load is predominantly transferred by friction in this stage (more than 90% of the total applied load). No plastic points are detected in this phase.
- At the mobilization phase, an obvious increase in the pile settlement rate occurs. The percentage of the load transferred by bearing increases in this phase. The soil skin friction also increases to achieve its peak value of the soil shear strength at pile settlement of 1.5% D. Plastic points are existed at the base and extended to a large part of the shaft.
- In the failure phase, the pile load transferred by friction tends to be constant or slightly decreases, and additional applied load is predominantly transferred by bearing. Apparent failure is often observed through the large induced pile settlement at the end of this stage. The plastic points existed at the base and covered almost the whole length on the pile shaft. In this study, the failure load of the large diameter bored pile could be identified with the size of the formed plastic bulb and/or the rate of settlement at the last loading increment;
  - The induced settlement at failure is greater than 1.5 times that at 90% of the ultimate load.
  - At the failure load, plastic zone fully covered the whole length of the pile shaft interface. Formed plastic bulb around the pile base has a size of about four times of pile diameter (4D) and extended below the pile base for a length of about three times (3D) of pile diameter.

REFERENCES

[1] M. W. O'Neill, and R. C. Reese (1999). Drilled Shafts: construction procedures and design methods. federal highway administration, Washington, d.c.

[2] M. Ezzat, M. Eid, A. Hefny, T. Sorour and Y. Zaghloul, Numerical Analysis of Large Diameter Bored Pile Installed in Multi Layered Soil: A Case Study of Damietta Port New Grain Silos Project, (2019). (Online) Inpressco.com. Available at: http://inpressco.com/wp-content/uploads/2018/03.

[3] ECP 202/4. (2005). Egyptian code for soil mechanics – design and construction of foundations. Part 4, Deep foundations. The Housing and Building Research Center (HBRC), Cairo, Egypt.

[4] DIN 4014. (1990). German association for earthworks and foundation engineering, Deutsches Institute fur Normung, Berlin, Germany.

[5] AASHTO, LRFD Bridge Design Specification, (1998), SI units, Second Edition.

[6] H. Sommer, & P. Hammbach, (1974). Großpfahlversuche im Ton für die Gründung der Talbrücke Alzey. Der Bauingenieur Vol. 49: 310-317.

[7] G. G. Meyerhof (1986). "Theory and Practice of Pile Foundations". In proceedings of the International Conference on Deep Foundations, Beijing, vol. 2, pp. 177-186.

[8] G. Mullins, S. Dapp and P. Lai (2000). "Pressure Grouting Drilled Shaft Tips in Sand". New technological and design developments in deep foundations, N. D. Dennis, R. Castelli, and M. W. O'Neill, eds., ASCE, Reston.

[9] J. B. Hansen (1963). Discussion on hyperbolic stress-strain response in cohesive soils. ASCE, Vol. 89, SM4, pp. 241-242.

[10] F. K. Chin (1970). Estimation of the ultimate load of piles from tests not carried to failure. Proc., 2nd. South-East Asian Conf. on Soil Eng., Singapore, pp.81-90.

[11] F. M. El-Nahhas, Y. M. El-Mossallamy, and M. M. Tawfik, (2009), Assessment of the skin friction of large diameter bored piles in sand, Proceedings of the 17th International Conference on Soil Mechanics and Geotechnical Engineering.

[12] J. H. Lee and R. Salgado (1999). Determination of Pile Base Resistance in Sands. Journal of Geotechnical and Geoenvironmental Eng., ASCE, vol. 125, no. 8, pp. 673 683.

[13] Y. El-Mossallamy (1999). Load-settlement behaviour of large diameter bored piles in over-consolidated clay. Proceeding of the 7th. International Symposium on Numerical Models in Geotechnical Engineering, Graz, Austria, September 1999, pp. 443-450.

[14] R. O. Davis, K. C. Change, and G. Mullenger (1989). Modeling of axially loaded piles: comparisons with pile test load. Computer and physical modeling in geotechnical, Rotterdam.

[15] S. V. Baars & W. V. Niekerk (1999). Numerical modelling of tension piles. In International Symposium on Beyond 2000 in Computational Geotechnics, pp. 237-246.

[16] H. Meibner, H. Shen and W. F. Van Impe (1993). Punching effects for bored piles. Conference on Deep Foundations and Auger Piles, Rotterdam.

[17] M. Wehnert and P. A. Vermeer (2004). Numerical Analyses of Load Tests on Bored Piles. Numerical Models in Geomechanics. NUMOG 9th. Ottawa, Canada.

[18] J. B. Burland (1965). The Yielding and Dilating of Clay. (Correspondence) Géotechnique Vol. 15: 211-214.

[19] R. B. Brinkgreve and P. A. Vermeer (1999). Edition manual of PLAXIS. Blkema, Rotterdam, Brookfield

[20] J. Ohde (1939). Zur Theorie der Druckverteilung im Baugrund.Der Bauingenieur Vol. 20: 451-459.

[21] N. Janbu (1963). Soil compressibility as determioned by oedometer and triaxial tests. Proc. ECSMFE, Wiesbaden, Vol. 1:19-25.

[22] A. E. Groen (1995), Elastoplastic Modelling of Sand Using a Conventional Model. Tech. Rep. 03.21.0.31. 34/35, Delft University of Technology.

[23] Fitsum Teshome & Araz Ismail, (2011), Analysis of deformations in soft clay due to unloading. Master's Thesis, Department of Civil and Environmental Engi-neering Division of GeoEngineering, Chalmers Uni.

[24] F. H. Kulhawy and P. W. Mayne (1989), "Manual on estimating soil properties for foundation design." Rep. No. EPRI EL-6800, Electric Power Research Institute, Palo Alto, Calif. 2–25.

[25] MIDAS GTS NX user manual, Analysis Reference chapter 4 materials, Section 2. Plastic Material Properties.

[26] C. Moormann, (2002). Trag- und Verformungsverhalten tiefer Baugruben in bindigen Böden unter besonderer Berücksichtigung der Baugrund-Tragwerk- und der Baugrund- Grundwasser-Interaktion. Mitteilungen des Institutes und der Versuchsanstalt für Geotechnik der Technischen Universität Darmstadt: Heft 59.

[27] K. M. Rollins, R. J. Clayton, R. C. Mikesell and B.C. Blaise (2005), Drilled Shaft Side Friction in Gravelly Soils. Journal of Geotechnical and Geoenvironmental Engineering, Vol. 131, No. 8, pp. 987-1003.

[28] E. Franke (1976). Pile foundations – single piles. Proceedings of the 6th ECSMFE, Wien, Vol. 2.1: 83-102.

[29] F. T. Touma & L. C. Reese (1972). Behavior of bored piles insand. Proceedings of the ASCE Vol.100 NO.GT7: 749-761.